Thin Solid Films 791 (2024) 140218

Contents lists available at ScienceDirect

Thin Solid Films

journal homepage: www.elsevier.com/locate/tsf

Effect of substrate temperature on structure, morphology and optical properties of Sb_2Se_3 thin films fabricated by chemical-molecular beam deposition method from Sb and Se precursors for solar cells

T.M. Razykov [a], A. Bosio [b], K.M. Kouchkarov [a], R.R. Khurramov [a,*], M.S. Tivanov [c], D.S. Bayko [c], A. Romeo [d], N. Romeo [b]

[a] Physical-Technical Institute, Chingiz Aytmatov Street 2B, Tashkent 100084, Uzbekistan
[b] University of Parma, G. P Usberti 7/A, Parma 43124, Italy
[c] Faculty of Physics, Belarusian State University, Minsk 220030, Belarus
[d] Universita' di Verona, Ca' Vignal 2- Strada Le Grazie 15, Verona 37134, Italy

ARTICLE INFO

Keywords:
Antimony triselenide
Chemical molecular beam deposition
Raman spectroscopy

ABSTRACT

Sb_2Se_3 thin films were obtained by chemical-molecular beam deposition on soda-lime glass from high purity Sb and Se precursors at 400 °C, 450 °C and 500 °C substrate temperature. Due to the precise control of the Sb/Se ratio, Sb_2Se_3 thin films with stoichiometric composition were obtained, which was confirmed by energy-dispersive X-ray microanalysis. The effect of substrate temperature on morphology, structure and optical properties of Sb_2Se_3 thin-films were studied by scanning electron microscopy, atomic force microscopy, X-ray diffraction, Raman spectroscopy and from the analysis of absorption and transmission spectra of the films. Average diameters and lengths of Sb_2Se_3 rods deposited at different substrate temperature were the range of 0.5–2 μm and 1–4 μm respectively which was grown at different slope and compactness to the substrate. The optical bandgap of the films was determined from the transmission and reflection spectra and 1.16, 1.21 and 1.26 eV band gap energies were observed for 500, 450 and 400 ℃ substrate temperature Sb_2Se_3 thin films respectively.

1. Introduction

Over the last years, as the interest in Sb_2Se_3 chalcogenide thin films became stronger, researchers devoted to the synthesis of this compound have doubled in the recent decade. Studies showed that this binary compound has good electrochemical, optoelectric properties. The direct bandgap of this material for a single-junction solar element is between 1.1 and 1.3 eV [1] and strong absorption of sunlight $\alpha > 10^5\ cm^{-1}$ in the visible spectra [2], carrier mobility $\approx 10\ cm^2V^{-1}s^{-1}$ for minority carriers and based on the transient absorption spectroscopy, a carrier lifetime ≈ 60 ns [3]. In addition, the elements that make up these materials have a relatively low cost, with amphibious Sb and Se with contents of 0.2 and 0.05 ppm (parts per million), respectively, resistance to external influences and nontoxicity [4]. According to the electrochemical properties, Sb_2Se_3 has been suggested as an anode material for lithium-ion batteries [5] and higher initial hydrogen storage capacity material [6]. Sb_2Se_3 binary compound is used in optical recording material [7], in thermoelectric devices [8], solar cells and photoelectrochemical cell [9] applications due to excellent optoelectronic properties. At present, the efficiency of thin film solar cells based on Sb_2Se_3 is 10.57 % [10]. However, the theoretically calculated efficiency of Sb_2Se_3 solar cells can exceed 31 % by the ideal Shockley-Queisser limit [11]. The efficiency of Sb_2Se_3 solar cell is highly dependent on the physical properties of the base layer as well as the growth method. Among Sb_2Se_3 thin-film growth technology, the most common are rapid vacuum thermal evaporation [12], ionic layer adsorption and reaction methods [13], magnetron sputtering [14], chemical bath deposition [15], pulsed laser deposition [16], but all these methods required additional processes to improve the physical properties, such as selenization and subsequent annealing (structural, morphological and optical) of the absorbing layer. In our method, we can obtain different compositions of thin films without additional procedures by changing the temperature of the precursors during growth. Recently, we described fabrication of Sb_2Se_3 films by chemical-molecular beam deposition (CMBD) method [17] and

* Corresponding author.
E-mail address: rkhurramov@yahoo.com (R.R. Khurramov).

https://doi.org/10.1016/j.tsf.2024.140218
Received 13 June 2023; Received in revised form 28 December 2023; Accepted 9 January 2024
Available online 13 January 2024

discussed their characteristics in [18]. Structure, morphology and optical properties of Sb_2Se_3 films fabricated at substrate temperatures of 400 °C, 450 °C and 500 °C are discussed in this paper.

2. Experimental

Sb_2Se_3 thin films were deposited on soda-lime glass (SLG). The SLG substrates were cleaned using detergent, deionized water, acetone, and ethanol in an ultrasonic cleaning bath and N_2 gas drying in sequence. Sb_2Se_3 films were deposited by CMBD processes using two different quartz crucibles each loaded with Sb (99.999 % purity) or Se (99.99 % purity) beads. Quartz crucibles were positioned to heat treatment from special temperature-controlled molybdenum heaters, and Sb and Se granules were melted and evaporated from the crucibles at atmospheric pressure with gaseous hydrogen at a flow rate of 20 cm^3 /min. The SLG substrates were placed at the top of reaction camera by molybdenum holder mask which was further detailed our previous works [17,18]. We put an additional thermocouple to the substrate for monitoring the exact temperature. At 400, 450 and 500 °C substrate temperatures Sb_2Se_3 thin films were obtained at Sb 900–960 °C and Se 400–500 °C with a 30 min evaporation time. We limited Sb_2Se_3 thin films substrate temperature from 400 °C to 500 °C since to keep away from thermal damage the SLG substrates (<540 °C) and poor quality crystallization of Sb_2Se_3 thin films at temperature below 400 °C. It should also be noted that when heated above 500 °C, there is a deficiency of selenium in films, which leads to an increase in the number of defects and a deviation of the phase composition of films from stoichiometry. As a consequence, when using such films in photovoltaics applications, it leads to an increase in the number of recombination centers and decrease open-circuit voltage [19].

The reactor was naturally cooled down after film deposition. The average 2 μm thickness of the thin films was determined using a metallographic vertical microscope MIM-7 (POCC).

The morphological, structural and optical properties of Sb_2Se_3 thin films were analysed by various techniques. The chemical compositions of different substrate temperature samples were determined by energy dispersive X-ray (EDX) analysis using an Aztec Energy Advanced X-Max 80 (Oxford Instruments) spectrometer with an accelerating voltage of 20 kV and an estimated penetration depth of about 1.6 microns. The surface morphology, average grain size and topography of the films were investigated by using a LEO-1455 VP (Carl Zeiss) scanning electron microscope (SEM) operating voltage used for imaging is 20 kV and a Solver Nano (NT-MDT) atomic force microscope (AFM). The AFM instrument was used in the semi-contact mode, with a scanning probe of 10 nm tip radius, at a resonance frequency of 236 kHz. The crystal structure was performed by using an Ultima IV (Rigaku) X-ray diffractometer in the grazing incidence diffraction geometry at 1° of incident X-rays with CuKα radiation source (λ = 1.54178 Å). X-ray diffraction (XRD) analysis was carried out with the use of the database of the Joint Committee on Powder Diffraction Standard (JCPDS) and Crystallography Open Database (COD). Regarding structure analysis, Raman spectra were measured at room temperature, using a Nanofinder HE (LOTIS TII) confocal spectrometer with spectral resolution was better, than 2.5 cm^{-1}. A solid-state laser, with a radiation wavelength of 532 nm, was used to excite. The power of laser radiation incident on the samples was reduced to 60 μW, to avoid thermal damage. The size of the area, on which the laser radiation was focused on the surface of the samples, was about 0.7 μm in diameter. The optical properties of the films were acquired by a spectrophotometer Photon RT (Essent Optics) in the wavelength range of 400–3000 nm with spectral resolution better than 5 nm using unpolarized light at room temperature.

3. Results and discussions

Firstly, we characterized the chemical compositions of samples by EDX analysis and the stoichiometric ratio Sb_2Se_3 films deposited at 400 °C, 450 °C and 500 °C substrate temperature were obtained. An example of a typical EDX spectrum is shown in Fig. 1.

The surface morphology and grain size of rods were investigated by using SEM results. The structure of Sb_2Se_3 thin films is an array of randomly arranged rods (Fig. 2), which, depending on the temperature of the substrate. Average diameters and lengths of Sb_2Se_3 rods deposited at different substrate temperature were the range of 0.5–2 μm and 1–4 μm respectively which was grown at different slope and compactness to the substrate.

The crystal structure is formed by $(Sb_4Se_6)_n$ ribbons stacked in parallel in the [001] film depth direction through strong covalent Sb–Se bonds [20,21]. In general, the surface morphology of pure Sb_2Se_3 demonstrates from fine to coarse grain structures during grain growth as the substrate temperature increases.

To further study the morphology of Sb_2Se_3 thin films, AFM measurements were performed. Fig. 3 shows the AFM images of Sb_2Se_3 thin films. All AFM parameters for the different substrate temperature Sb_2Se_3 thin films are given in Table 1. Studies conducted using AFM showed that the thin films have a highly developed surface relief. The value of the average surface roughness Sa is in the range of ~0.1–0.4 μm. The average and root mean-square roughness of thin films surface increases with the increase of substrate temperature, while the surface skewness decreases from the characteristic values of the normal distribution (zero skewness reflects symmetrical height distribution) to a value of 0.44. These AFM results indicated that the grain size of thin films enlarges with the substrate temperature increases. The roughening of the surface can be explained by a complex process. When the substrate temperature raises the critical radius of nucleus of grains is growing and it is explained by Gibbs free energy [22]. This, as well as structural features of $(Sb_4Se_6)_n$ ribbons, lead to the fact that at temperatures within 350–400 °C the growth of crystallites with an orientation of type (hk0) prevails parallel to the substrate, and when heated, the proportion of crystallites growing at an angle to the base increases [23,24].

XRD analysis was carried out by Rigaku Ultima IV diffractometer. The results showed that all thin films have noticeable peaks that are in good agreement with the standard JCPDS map (No. 15–0861) of the Sb_2Se_3 orthorhombic phase. Thin films deposited at substrate temperatures of 450 ℃ and 500 ℃ crystallite peaks with the preferred orientation (hk1) are dominant, which are attributed to vertically oriented ribbons. Among the orientations (hk1), the preferred orientations (211) and (221) became more intense. (hk1)-Oriented grains, consisting of $(Sb_4Se_6)_n$ ribbons, have a certain angle of inclination with the substrate, which has the best carrier transport ability. At 400 ℃ substrate temperature, dominant peaks had (hk0) orientation (Fig. 4a). The most intense peak for this sample with orientation (061) was not considered, since it is not possible to resolve it from the peak with orientation (360).

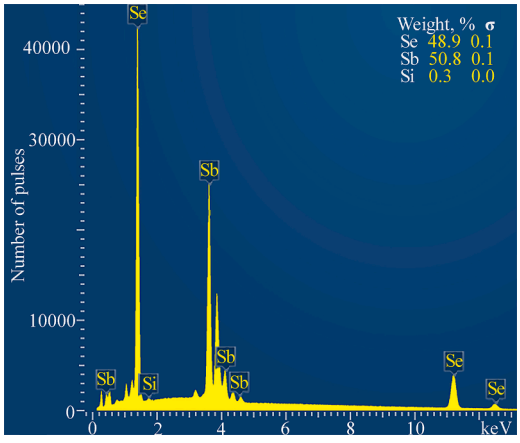

Fig. 1. A typical EDX spectrum.of Sb_2Se_3 thin films deposited at 500 ℃ substrate temperature.

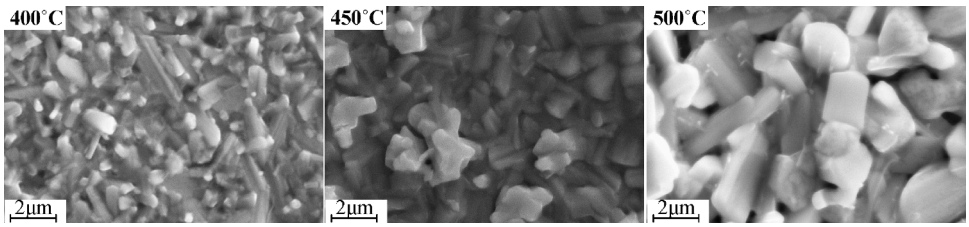

Fig. 2. Surface morphology of Sb_2Se_3 thin films deposited at different substrate temperatures.

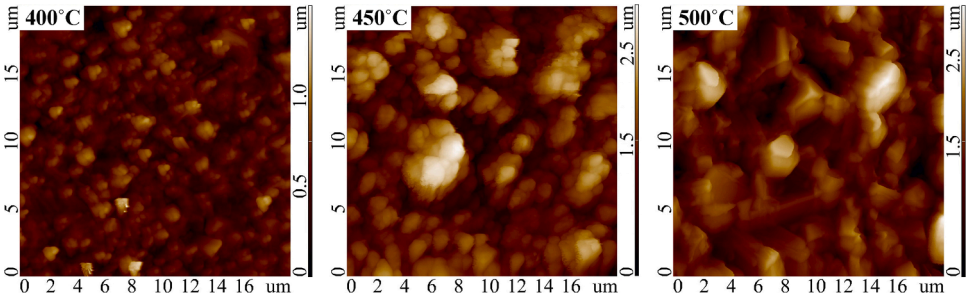

Fig. 3. AFM images of Sb_2Se_3 thin films deposited at different substrate temperatures.

Table 1
Surface roughness parameters of Sb_2Se_3 thin films deposited at different substrate temperatures.

$T_{substrate}$	400 ℃	450 ℃	500 ℃
Roughness average Sa, um	0.16	0.37	0.43
Root Mean Square Roughness Sq, um	0.22	0.48	0.55
Skewness Ssk	0.93	0.94	0.44
Kurtosis Ska	4.97	4.25	3.08

According to JCPDS map (No. 15–0861), the difference between the peaks is less than 0.3°. Orientation of crystallites of thin films is critically important for ensuring efficient charge transfer in a photoactive layer, since due to structural features, a strong directional anisotropy of electrooptical properties [24–26]. Zhou et al. found that in Sb_2Se_3 thin films, the high current part corresponds to the grain position of the film, while the low current part corresponds to the grain boundary, which indicates that carriers in Sb_2Se_3 thin films are mainly conducted through grains [27].

Raman scattering spectra were measured (Fig. 4b). to obtain additional information about the structural properties of Sb_2Se_3 films obtained by CMBD at different substrate temperatures with a stoichiometric composition of Sb/Se = 0.66. As can be seen from Fig. 4, the Raman spectra for all films show peaks characteristic of Sb_2Se_3:78, 83, 100, 122, 129, 153, 190, 211, 237 cm^{-1} [28]. The peaks at 153, 237 cm^{-1}, which are characteristic of Sb and trigonal Se, are also observed. But, the Raman peak at about 153 cm^{-1} is assigned to the characteristic of both Sb and Sb_2Se_3 [29,30]. Thus, the Raman results allow us to speak about the formation of the main phase Sb_2Se_3 and the secondary phase Sb, Se on the films. The emergency of secondary phases is a result of the flux deviations from appropriate proportion of Sb and Se contents from separate sources on the deposition process.

The absorption coefficient (α) of Sb_2Se_3 thin films was determined *via* transmission (T) and reflection (R) spectra (Fig. 5a) [18]. As widely known, the absorber layer bandgap for band-to-band direct allowed transitions can be determined by the dependence of the absorption coefficient on the photon energy in the Tauc plot which is described in the equation as below:

$$(\alpha h\nu)^2 = A\left(h\nu - E_g\right) \quad (1)$$

1.16, 1.21 and 1.26 eV band gap energies were observed for 500, 450 and 400 ℃ substrate temperature Sb_2Se_3 thin films respectively (Fig. 5b). These values of band gap are nearly similar with pure Sb_2Se_3 thin film (1.15 eV) [31]. A slight change in the band gap for three different substrate temperature Sb_2Se_3 thin films is an accordance with the change of thickness of the rods in relation to the bulk.

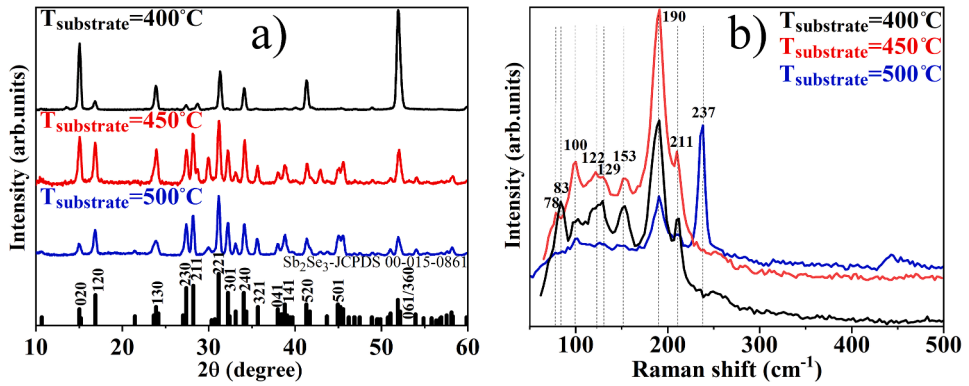

Fig. 4. X-ray patterns (a) and Raman spectra (b) of Sb_2Se_3 thin films obtained at different substrate temperatures.

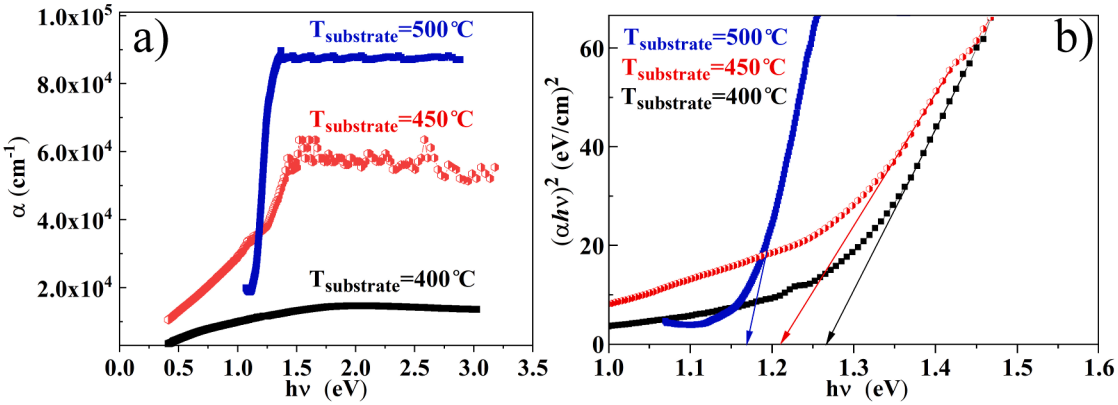

Fig. 5. Dependence of the absorption coefficient spectra α (a) and optical band gaps on the quantum energy (b) of Sb_2Se_3 films obtained at different substrate temperatures.

4. Conclusion

In this study, we have grown Sb_2Se_3 thin films with different substrate temperature from separate sources of Sb and Se by the CMBD method and investigated the effect of substrate temperature to the morphological, structural and optical properties of them as the absorber materials for the photovoltaic absorber applications. From the SEM and AFM analysis, it was observed that the size of grains on films and average surface roughness enlarged slightly with the increase of substrate temperature. Thin films deposited at substrate temperatures of 450 ℃ and 500 ℃ crystallite peaks with the preferred orientation (hk1) were dominant, which are attributed to vertically oriented ribbons, while at 400 ℃ substrate temperature, dominant peaks had (hk0) orientation. The Raman spectra for all films showed the peaks of Sb-Se bonding. An analysis of the dependency functions $(\alpha h\nu)^2 = f(h\nu)$ showed suitable direct bandgap for different substrate temperature Sb_2Se_3 thin films.

CRediT authorship contribution statement

T.M. Razykov: Conceptualization, Formal analysis, Methodology, Project administration, Supervision, Writing – original draft. **A. Bosio:** Formal analysis, Methodology. **K.M. Kouchkarov:** Formal analysis, Methodology, Writing – original draft. **R.R. Khurramov:** Data curation, Formal analysis, Investigation, Visualization, Writing – original draft, Writing – review & editing. **M.S. Tivanov:** Conceptualization, Visualization, Writing – review & editing. **D.S. Bayko:** Investigation, Visualization. **A. Romeo:** Writing – review & editing. **N. Romeo:** Writing – review & editing.

Declaration of competing interest

The authors declare the following financial interests/personal relationships which may be considered as potential competing interests:

R.R. Khurramov reports financial support was provided by the Ministry of innovative development of the Republic of Uzbekistan (Grant No: MRB-2021–540) and the State Committee on Science and Technology of the Republic of Belarus (Grant No: F21UZBG-022).

Data availability

No data was used for the research described in the article.

Acknowledgments

This work was supported by the Ministry of innovative development of the Republic of Uzbekistan (Grant No: MRB-2021-540) and the State Committee on Science and Technology of the Republic of Belarus (Grant No: F21UZBG-022).

References

[1] K. Li, F. Li, C. Chen, P. Jiang, S. Lu, S. Wang, Y. Lu, G. Tu, J. Guo, L. Shui, Z. Liu, B. Song, J. Tang, One- dimensional Sb_2Se_3 enabling ultra-flexible solar cells and mini-modules for IoT applications, Nano Energy 86 (2021) 106101.
[2] Y. Zhou, M. Leng, Z. Xia, J. Zhong, H. Song, X. Liu, B. Yang, J. Zhang, J. Chen, K. Zhou, J. Han, Y. Cheng, J. Tang, Solution-processed antimony selenide heterojunction solar cells, Adv. Energy Mater. 4 (8) (2014) 1301846, https://doi.org/10.1002/aenm.201301846.
[3] N. Spalatu, R. Krautmann, A. Katerski, E. Karber, R. Josepson, J. Hiie, I.O. Acik, M. Krunks, Screening and optimization of processing temperature for Sb_2Se_3 thin film growth protocol: interrelation between grain structure, interface intermixing and solar cell performance, Sol. Energy Mater. Sol. Cells 225 (2021) 111045, https://doi.org/10.1016/j.solmat.2021.111045.
[4] K. Zeng, D.J. Xue, J. Tang, Antimony selenide thin-film solar cells, Semicond. Sci. Technol (2016), https://doi.org/10.1088/0268-1242/31/6/063001.
[5] M.-Z. Xue, Z.-W. Fu, Pulsed laser deposited Sb_2Se_3 anode for lithium-ion batteries, J. Alloys Compd. 458 (1) (2008) 351–356.
[6] J. Ma, Y. Wang, Y. Wang, Q. Chen, J. Lian, W. Zheng, Controlled synthesis of one dimensional Sb_2Se_3 nanostructures and their electrochemical properties, J. Phys. Chem. C 113 (31) (2009) 13588–13592.
[7] Y. Nakane, N. Sato, H. Makinon, S. Miyaoka, Principle of laser recording mechanism by forming an alloy in the multilayer of thin metallic films, in: Proceedings of the SPIE 0529, Optical Mass Data Storage I, 1985, p. 76.
[8] H.C. Kim, T.S. Oh, D.-B. Hyun, Thermoelectric properties of the p-type Bi_2Te_3-Sb_2Te_3- Sb_2Se_3 alloys fabricated by mechanical alloying and hot pressing, J. Phys. Chem. Solids 61 (5) (2000) 743–749.
[9] B.R. Sankapal, C.D. Lokhande, Studies on photoelectrochemical (PEC) cell formed with SILAR deposited Bi_2Se_3 – Sb_2Se_3 multilayer thin films, Sol. Energy Mater. Sol. Cells 69 (1) (2001) 43–52.
[10] Y. Zhao, Sh. Wang, Ch. Li, B. Che, X. Chen, H. Chen, R. Tang, X. Wang, G. Chen, T. Wang, J. Gong, T. Chen, X. Xiao, J. Li, Regulating deposition kinetics *via* a novel additive-assisted chemical bath deposition technology enables fabrication of 10.57%- efficiency Sb_2Se_3 solar cells, Energy Environ. Sci. (2022), https://doi.org/10.1039/d2ee02261c.
[11] S. Rühle, Tabulated values of the Shockley-Queisser limit for single junction solar cells, Solar Energy 130 (2016) 139–147, https://doi.org/10.1016/j.solener.2016.02.015.
[12] S. Rijal, D. Li, R.A. Awni, Ch. Xiao, S.S. Bista, M.K. Jamarkattel, M.J. Heben, Ch. Jiang, M. Al-Jassim, Z. Song, Y. Yan, Templated growth and passivation of vertically oriented antimony selenide thin films for high-efficiency solar cells in substrate configuration, Adv. Funct. Mater. 32 (2022) 2110032, https://doi.org/10.1002/adfm.202110032.
[13] C.D. Lokhande, B.R. Sankapal, S.D. Sartale, H.M. Pathan, M. Giersig, V. Ganesan, A novel method for the deposition of nanocrystalline Bi_2Se_3, Sb_2Se_3 and Bi_2Se_3-Sb_2Se_3 thin films SILAR, Appl. Surf. Sci. 182 (3) (2001) 413–417.
[14] C. Ma, H. Guo, X. Wang, Z. Chen, Q. Cang, X. Jia, Y. Li, N. Yuan, J. Ding, Fabrication of Sb_2Se_3 thin film solar cells by co-sputtering of Sb_2Se_3 and Se targets, Solar Energy 193 (2019) 275–282, https://doi.org/10.1016/j.solener.2019.09.046.
[15] H. Maghraoui-Meherzi, T. ben Nasr, M. Dachraoui, Synthesis, structure and optical properties of Sb_2Se_3, Mater. Sci. Semicond. Process 16 (2013) 179–184, https://doi.org/10.1016/j.mssp.2012.04.019.
[16] A. Mavlonov, A. Shukurov, F. Raziq, H. Wei, K. Kuchkarov, B. Ergashev, T. Razykov, L. Qiao, Structural and morphological properties of PLD Sb_2Se_3 thin

films for use in solar cells, Solar Energy 208 (2020) 451–456, https://doi.org/10.1016/j. solener.2020.08.004.
[17] T.M. Razykov, A. Bosio, B.A. Ergashev, D. Isakov, R. Khurramov, K.M. Kouchkarov, M.A. Makhmudov, A. Romeo, N. Romeo, M.S. Tivanov, Sh.B. Utamuradova, D. S. Bayko, L.S. Lyashenko, O.V. Korolik, A.A. Mavlonov, Structural and optical properties of Sb_xSe_y thin films obtained by chemical molecular beam deposition method from Sb and Se precursors, Solar Energy 254 (2023) 67–72, https://doi.org/10.1016/j.solener.2023.03.010.
[18] T.M. Razykov, K.M. Kuchkarov, M.S. Tivanov, D.S. Bayko, L.S. Lyashenko, B. A. Ergashev, A. Mavlonov, A.N. Olimov, R. Khurramov, D.Z. Isakov, M. Pirimmatov, Characteristics of thin Sb_2Se_3 films obtained by the chemical molecular beam deposition method for thin-film solar cells, Thin Solid Films 774 (2023) 139844, https://doi.org/10.1016/j.tsf.2023.139844.
[19] S. Chen, X. Hu, J. Tao, J. Xue, G. Weng, J. Jiang, X. Shen, Sh. Chen, Effects of substrate temperature on material and photovoltaic properties of magnetron-sputtered Sb_2Se_3 thin films, Appl. Opt. 58 (2019) 2823–2827.
[20] D. Wang, C. Song, X. Fu, X. Li, Growth of one-dimensional Sb_2S_3 and Sb_2Se_3 crystals with straw-tied-like architectures, J. Cryst. Growth 281 (2005) 611–615, https://doi.org/10.1016/j.jcrysgro.2005.04.064.
[21] V.L. Deringer, R.P. Stoffel, M. Wuttig, R. Dronskowski, Vibrational properties and bonding nature of Sb_2Se_3 and their implications for chalcogenide materials, Chem. Sci. 6 (2015) 5255–5262.
[22] S.N. Park, S.Y. Kim, S.J. Lee, Sh.J. Sung, K.J. Yang, J.K. Kang, D.H. Kim, Controlled synthesis of (hk1) preferentially oriented Sb_2Se_3 rod arrays by co-evaporation for photovoltaic applications, J. Mater. Chem. A (2019), https://doi.org/10.1039/c9ta08289a.
[23] S. Rijal, D. Li, R. Awni, S. Bista, Z. Song, Y. Yan, Influence of post-selenization temperature on the performance of substrate-type Sb_2Se_3 solar cells, ACS Appl. Energy Mater. 4 (5) (2021) 4313–4318, https://doi.org/10.1021/acsaem.1c00657.
[24] D. Ren, X. Luo, Sh. Chen, Z. Shuo, C. Zhuanghao, L. Michel, M. Guangxing, Q. Hongli, F. Xvsheng, Z. Xianping, X. Hua, Structure, morphology, and photoelectric performances of Te-Sb_2Se_3 thin film prepared *via* magnetron sputtering, Nanomaterials 10 (2020) 1358, https://doi.org/10.3390/nano10071358.
[25] Z. Li, X. Liang, G. Li, H. Liu, H. Zhang, J. Guo, J. Chen, K. Shen, X. San, W. Yu, 9.2%-efficient core-shell structured antimony selenide nanorod array solar cells, Nat. Commun. 10 (2019) 1–9, https://doi.org/10.1038/s41467-018-07903-6.
[26] K. Li, R. Tang, Ch. Zhu, T. Chen, Critical review on crystal orientation engineering of antimony chalcogenide thin film for solar cell applications, Adv. Sci. (2023) 2304963, https://doi.org/10.1002/advs.202304963.
[27] J. Zhou, H. Chen, X. Zhang, K. Chi, Y. Cai, Y. Cao, J. Pang, Substrate dependence on $(Sb_4Se_6)_n$ ribbon orientations of antimony selenide thin films: morphology, carrier transport and photovoltaic performance, J. Alloys Compd. 862 (2021) 158703, https://doi.org/10.1016/j.jallcom.2021.158703.
[28] V.F. Pedro, G. Maxim, A. Xavier, J. Tariq, P. Marcel, Multiwavelength excitation Raman scattering study of Sb_2Se_3 compound: fundamental vibrational properties and secondary phases detection, 2d Mater. 6 (2019), https://doi.org/10.1088/2053-1583/ab4029/.
[29] A. Kumar, V. Kumar, A. Romeo, C. Wiemer, G. Mariotto, Raman spectroscopy and *in situ* XRD probing of the thermal decomposition of Sb_2Se_3 thin films, J. Phys. Chem. C 125 (36) (2021) 19858–19865, https://doi.org/10.1021/acs.jpcc.1c05047.
[30] A. Shongalova, M.R. Correia, J.P. Teixeira, J.P. Leitão, J.C. González, S. Ranjbar, S. Garud, B. Vermang, J.M.V. Cunha, P.M.P. Salomé, P.A. Fernandes, Growth of Sb_2Se_3 thin films by selenization of RF sputtered binary precursors, Sol. Energy Mater. Sol. Cells 187 (2018) 219–226, https://doi.org/10.1016/j.solmat.2018.08.003.
[31] C. Chen, W. Li, Y. Zhou, C. Chen, M. Luo, X. Liu, K. Zeng, B. Yang, C. Zhang, J. Han, J. Tang, Optical properties of amorphous and polycrystalline Sb_2Se_3 thin films prepared by thermal evaporation, Appl. Phys. Lett. 107 (2015), https://doi.org/10.1063/1.4927741.